Advanced Electronic Materials

ADVANCED ELECTRONIC MATERIALS Open Access

www.advelectronicmat.de

RESEARCH ARTICLE OPEN ACCESS

Towards Real-Time Monitoring of Soft Robotic Systems in Endoscopic Application With Ultra-Flexible Organic Transistor-Based Strain Sensors

Usama Mahmood[1] | Andrea Bartolucci[2,3] | Giulia Casula[1] | Antonello Mascia[1] | Lorenzo Vannozzi[2,3] | Stefano Lai[1]

[1]Department of Electrical and Electronic Engineering, Department of Excellence, University of Cagliari, Cagliari, Italy | [2]The Biorobotics Institute, Scuola Superiore Sant'Anna, Pisa, Italy | [3]Department of Excellence in Robotics & AI, Scuola Superiore Sant'Anna, Pisa, Italy

Correspondence: Lorenzo Vannozzi (lorenzo.vannozzi@santannapisa.it) | Stefano Lai (stefano.lai@unica.it)

Received: 8 December 2025 | **Revised:** 3 April 2026 | **Accepted:** 28 April 2026

Keywords: inkjet printing | mechanical characterization | organic transistor | soft robotics | strain sensor

ABSTRACT

The development of sensing elements capable of direct and real-time monitoring is fundamental to the actual exploitation of soft robotic systems in real application scenarios. In this paper, the integration of an electronic strain sensor based on an ultra-flexible, all-organic field-effect transistor on a soft structure, conceived for future application as a soft robotic catheter in drug delivery, is reported. The device, entirely fabricated by means of cost-effective, large area processes, is developed over a sub-micrometrical, biocompatible substrate, with mechanical properties compatible with soft robotic production. Electrical performance of the transistor is characterized, showing the suitability of the device parameters to the envisaged application in terms of low power consumption and reproducibility. A successful integration of the ultra-flexible transistor platform into the soft robotic system is demonstrated. A thorough electromechanical characterization of the sensorized system is provided, showing a programmable sensitivity to mechanical deformation in the range 5°–30°, based on the overthreshold conditions imposed by the transistor gate voltage. The results pave the way for the effective exploitation of organic flexible electronics as a valuable solution for the development of sensorized soft robots, toward a complete observability and controllability of their actuation in operation scenarios.

1 | Introduction

Soft robotics has emerged as a transformative approach in biomedical engineering, offering compliant, deformable systems capable of safe and adaptive interaction with living tissues [1]. Unlike conventional rigid robots, soft robotic devices can conform to complex anatomical geometries and perform delicate manipulations with human-like dexterity in unstructured environments, making them highly suitable for applications such as minimally invasive surgery, rehabilitation, and physiological monitoring.

Early research on soft robotics primarily focused on the development of bioinspired designs and the exploration of various actuation technologies. Although researchers have investigated a wide range of actuators featured by fast response time and high energy density [2, 3], progress in the proprioceptive capabilities in soft robotics has lacked the same pace. The inherent softness that grants these robots their compliance poses a fundamental challenge: the lack of accurate and reliable sensing capabilities to perceive and control deformation, contact forces, and environmental interactions in real-time. For example, the lack

Usama Mahmood and Andrea Bartolucci contributed equally to this work.

of perception remains one of the major limiting factors that is hindering the development of safe, accurate, and efficient soft robot-assisted interventions in medical robotics [4].

Despite the inherent adaptability and flexibility of soft robots, predicting the dynamic behavior of soft materials is considerably more complex than modeling the kinematics of rigid joints, posing significant challenges in controlling and monitoring the shape and position of specific parts of soft robots [5]. One potential approach involves the use of morphological computation of programmable soft materials [6, 7], but achieving reliable control and monitoring remains challenging.

The integration of sensors into soft robots is essential to enhance the accuracy and efficiency of their control. However, sensors should ideally combine mechanical compliance to avoid interfering with robot performance, compact dimensions to preserve a wide range of motion, high durability across thousands of deformation cycles, and resistance to specific environments (ranging from delicate surgical settings to harsh rescue scenarios). The large deformations and versatile topologies of soft robots preclude the use of conventional sensors, such as encoders, which are well-suited for rigid robots.

Sensor design for soft robots represents a challenging problem, being at the same time the stage for the investigation of a broad range of critical parameters, including geometry, material, and actuation type [8]. Different approaches have been explored depending on the sensing modality, including optical, resistive, piezoresistive, magnetic, and capacitive techniques [9–14]. Among these, the most common strategy involves the embedding of stretchable strain sensors into the soft robotic structure, which can convert morphological changes into measurable signals. Nevertheless, the integration of such sensors can compromise the robot's performance, as the introduction of relatively stiff elements may reduce the inherent flexibility of the soft structure [15]. Indeed, the seamless integration of sensors within soft structures remains a current pivotal challenge in the field. Flexible and stretchable electronic sensors provide a promising solution to this limitation. Their ability to conform to curved and dynamic surfaces while maintaining electrical functionality allows them to be directly integrated into soft robotic structures without compromising mechanical performance. Recent studies have demonstrated that embedding or laminating such sensors onto soft actuators enables continuous monitoring of strain, pressure, or tactile feedback, which can be leveraged to improve control accuracy and enable closed-loop operation in biomedical contexts [16–18]. A great effort is being paid towards the development of new frameworks for the standardization of such approaches to assess mechanical and biological compatibility while keeping effective sensor features in terms of performance, montage, and readout, and overall cost-effectiveness.

In this work, the design, fabrication, and experimental characterization of a soft robotic platform hosting a flexible electronic strain sensor is presented. The proposed system (Figure 1) exploits the technology of ultra-flexible organic electronics to preserve the mechanical compliance of the overall platform, conceived as a tubular hollow element for the development of a soft robotic catheter to be employed in endoscopic drug delivery. In particular, the sensing element is an all-organic field-effect transistor entirely fabricated onto a 2 μm-thick, biocompatible substrate by means of large-area fabrication approaches. The choice for a transistor-based strain sensor enables the tunability of the sensitivity to deformation [19], thus enhancing the platform's capability to adapt to application and experimental conditions. All these aspects are unprecedented in the field of mechanical monitoring of soft robots, thus making the proposed approach completely innovative for both soft robotics and flexible organic electronics application field. The integration strategy ensures strong interfacial bonding between the sensor and the soft actuator, enabling the correct transfer of the deformation applied to the catheter in the transistor structure, which responds with a current signal proportional to the applied strain. A thorough mechanical and electromechanical characterization is reported, showing suitable performance of the sensorized soft robotic system for the development of the envisaged applications.

The results demonstrate the feasibility of combining flexible organic electronic sensors with soft robots to achieve precise, real-time monitoring of mechanical states relevant for biomedical tasks. In particular, the complete system is conceived to perform as a sensorized tip of a soft-robotic catheter in endoscopic applications, such as drug delivery. All in all, this work contributes to bridging the gap between flexible sensor technology and functional soft robotic systems, advancing their potential for applications in minimally invasive procedures, wearable therapeutic devices, and human–machine interfaces.

2 | Results and Discussion

2.1 | Sensors' Structure and Electrical Characterization

The strain sensor is an Organic Field-Effect Transistor (OFET), fully fabricated using large-area processes. The active structure of the device is entirely made of organic materials, with the sole exception of connecting routes and pads made of silver to ensure appropriate conductivity. A detailed description of the fabrication steps is provided in the Experimental Section. The device, as shown in Figure 1, has an interdigitated structure to enhance the aspect ratio while keeping the restrained area occupation to be compatible with the envisaged application. The whole device fabrication is carried out on a plastic support, to which the sensor substrate, i.e., a 500 nm-thick Parylene layer, is bonded by means of a sacrificial layer of polyvinyl alcohol (PVA). The ultra-flexible device is then released by a mechanical peel-off procedure, enabled by sacrificial frames, as detailed in the Experimental Section.

Preliminary to device integration into the soft robots, a detailed electrical characterization of the printed OFETs was performed. Representative transfer and output characteristics recorded in the saturation regime are shown in Figure 2. The transfer curves exhibited low hysteresis, indicative of good device stability, along with well-defined saturation behavior and threshold voltage compatible with low voltage operation. Leakage current (i.e., the current flowing through gate contact, I_G) is several orders of magnitude lower than direct current and independent from the gate voltage, thus clearly demonstrating the ideal properties of the insulator layer. The transistor operates in depletion mode,

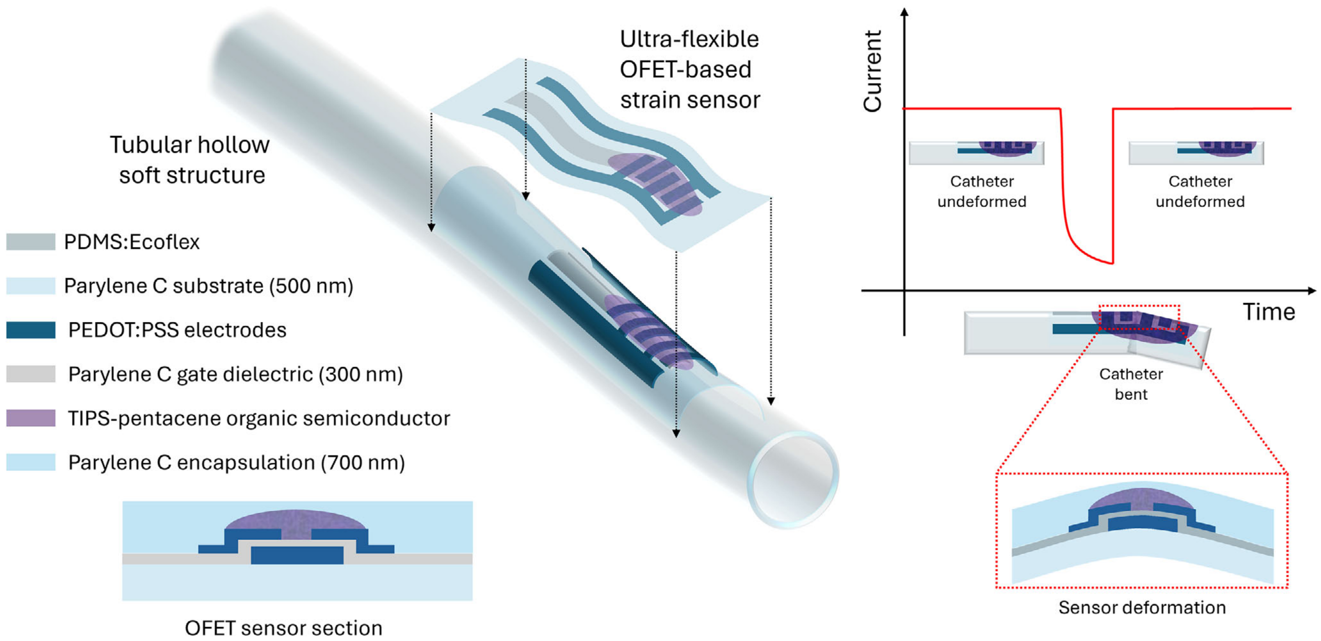

FIGURE 1 | The structure of the proposed soft robotic system with integrated sensor. Insets report the materials employed and the section of the OFET-based strain sensor, and a cartoon of the proposed working principle.

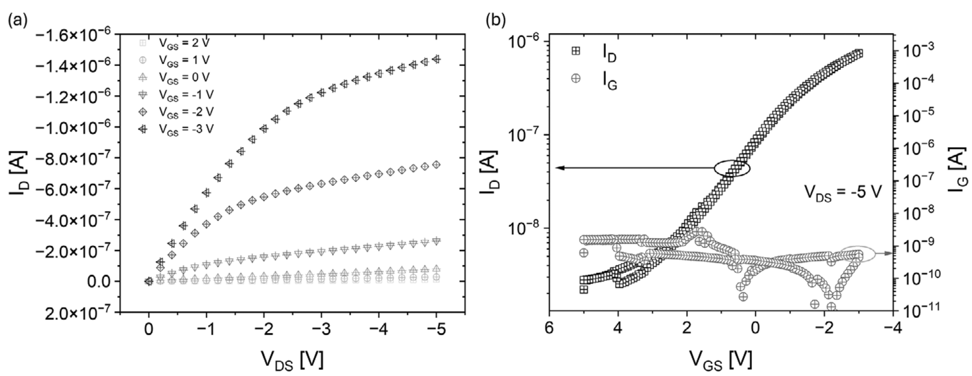

FIGURE 2 | Representative output (a) and transfer (b) current-to-voltage characteristics of ultra-flexible printed OFETs.

as already observed for Parylene-encapsulated OFETs [20]. The output characteristics demonstrated distinct triode and saturation regions with clear gate modulation, verifying proper transistor functionality. An overall process yield of about 98% was obtained.

Main electrical parameters were extrapolated by means of standard approaches from transfer characteristics in the saturation regime [21]. Average parameters, evaluated on a set of 15 devices, are summarized in Table 1.

TABLE 1 | Summary of electrical characteristics of ultra-flexible printed OFETs, including threshold voltage (V_{th}), field-effect mobility (μ), and average I_{on}/I_{off} ratio. Values represent the average $\pm$ 1-σ tolerance band calculated on a set of 15 devices.

Parameters	Value (average$\pm$1σ)
Threshold voltage [V]	1.1 ± 0.2
Charge carrier mobility [$cm^2V^{-1}s^{-1}$]	$(7 \pm 2)\cdot 10^{-2}$
On/off current ratio [a.u.]	$(1.7 \pm 1.0)\ 10^4$

2.2 | Sensor Integration on Soft Robotic Structure and Mechanical Characterization

Figure 3a shows the sensorized soft robotic system after the integration process. A detailed description of the lamination procedure and setup is provided in the Experimental Section and in (Figure S1). Briefly, a thin, uncured layer of silicone is used as a glue to promote an intimate bonding between the Parylene C substrate hosting the sensor and the soft robotic structure. Interestingly enough, the composition of the silicone blend used as glue is the same as that employed for the fabrication of the soft robotic structure, and this enhances adhesion stability

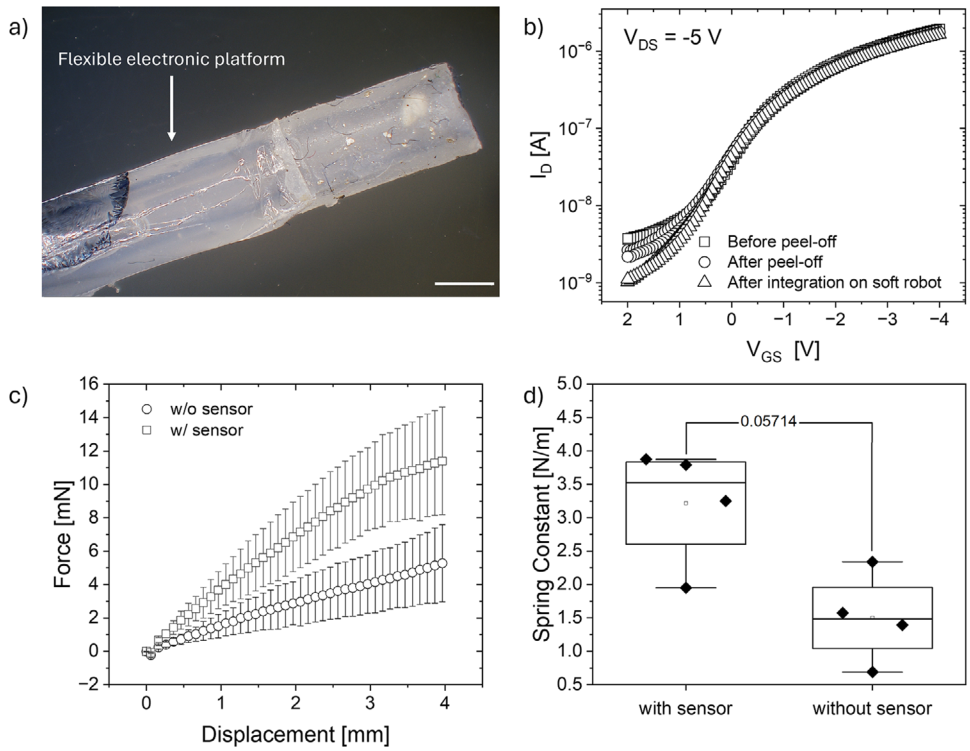

FIGURE 3 | Sensor integration and mechanical characterization: (a) Side view of a soft robotic structure with an integrated flexible electronic platform. Scale bar is 2 mm. (b) Transfer characteristic group of a device before (squares) and after (circles) the peel-off process, and after the integration on a soft robotic system (triangles). (c) Comparison of the force required to displace the soft robotic platform up to 4 mm, with and without the sensor. Curves represent the mean values of the samples analyzed ($N = 4$), with variability across samples indicated. (d) Comparison of the spring constant calculated from the force-displacement curves for the soft robotic structure with and without a sensor. Statistical significance was assessed using the Mann-Whitney test (p-value < 0.05), with $N = 4$ independent samples per group. Values are reported in boxplots.

through good chemical and interfacial compatibility and ensures a continuous conformability, as demonstrated in previous studies [22, 23]. Indeed, using an intermediate layer exhibiting mechanical properties between Parylene (stiffness: 0.58 GPa) [24] and the material of the soft robotic structure (mixture of PDMS and EcoFlex 00–10, stiffness: 0.11 MPa) [25] might not be appropriate if the adhesion between the elements is insufficient [8]. The introduction of an intermediate layer acting as an adhesive glue between the sensor and the robotic structure enabled a stable coupling between the elements, reducing the risk of delamination and maintaining more uniform deformability across the system. Optical inspection of the cross-section of sensorized catheter tips allowed demonstrating the formation of an intimate contact between the Parylene layer and the Ecoflex structure (Figure S2).

A successful integration of the sensing system into the soft robotic platform relies on (i) ensuring that the sensor's basic electrical functionality is not affected by the peel-off and lamination steps, (ii) demonstrating that the overall soft robotic system stiffness is not affected by the ultra-flexible sensor. Figure 3b reports a representative transfer characteristic curve of an OFET sensor on support (squares), after the peel-off in its free-standing state (circles) and after the lamination procedure (triangles): it is possible to observe that any significant variation in the device characteristics has been observed during the whole process; average relative variation on electrical parameters (evaluated on 8 samples) is reported in Figure S3.

Mechanical analysis of the soft robotic platform integrated with the flexible sensor was conducted to assess the influence of sensor integration on the bending behavior of the structure. The analysis quantified the force required to achieve a bending angle of approximately 30° by applying a controlled displacement of 4 mm at a point located 7.5 mm from the constrained extremity of the soft robotic structure (Figure S4). The resulting force–displacement curves for both the standalone soft robotic platform and the integrated system are reported in Figure 3c. For the fully integrated system, a median value of approximately 12.27 mN was required to achieve 4 mm of displacement, while the soft robotic platform alone required about 5.40 mN to achieve the same displacement. It is also worth mentioning that no evidence of buckling or kinking was observed across all test conditions, which is a critical aspect involving a hollow soft robotic cylindrical structure made of silicone, which is featured by a Poisson's ratio close to 0.5 [26].

The integration of an on-board sensor within a soft robotic structure inherently alters its mechanical response, as it modifies the stiffness distribution within the system. The inclusion of the electronic platform can reduce the deformability of soft robotic structures by introducing additional rigidity. In particular, the sensor may increase the flexural rigidity, as Parylene C exhibits a Young's modulus almost three orders of magnitude higher than that of silicones, despite the relatively thin thickness [27]. As a result, the force needed to displace the integrated system shifted toward higher values, potentially reducing force sensitivity.

In other words, for an equivalent mechanical input, the OFET output signal is expected to decrease compared with that of the bare soft robotic platform.

However, the experimental results presented in Figure 3d indicate that the spring constants calculated for the soft robotic structure, with and without a sensor, did not exhibit statistically significant differences. Although no statistically significant differences were observed, an increase in the median spring constant (from 1.49 to 3.52 N/m) was measured upon sensor integration, indicating a moderate stiffening effect. This behavior was attributed to the higher stiffness of the sensing layer, while its ultra-thin nature and partial coverage (covered surface∼50%) minimized the stiffening effect.

Indeed, approximating the catheter as a hollow cylindrical beam, a first-order estimation of the flexural rigidity (EI) with the beam theory for soft robotic silicone structure alone is 1.6×10^{-7} Nm^2, while the addition of a thin Parylene C layer, assuming full circumferential coverage and perfect bonding, would lead to a value of 6.0×10^{-6} Nm^2, corresponding to an increase of more than one order of magnitude. This configuration, however, represents an upper-bound scenario. In the actual system, the sensing layer was applied as partial coverage of the surface, and the overall mechanical response was dominated by the hyperelastic behavior of the silicone substrate undergoing large deformation. Under these conditions, the contribution of the stiff Parylene C layer remained localized, and its effect on the global flexural response was significantly reduced.

This confirms the initial hypothesis that integrating such a flexible electronic platform on the outer surface of an elastomeric matrix minimally alters its stiffness [15]. The configuration under analysis allows the mechanical coupling between the sensor and the soft structure to be tailored according to the specific application [28]. The strategic placement of the sensor over selected regions and minimization of the surface area covered by Parylene C could further mitigate its impact on stiffness, although a detailed investigation of this aspect lies beyond the scope of the present study.

While the experimental analysis highlights an increase in stiffness, expressed as spring constant, upon sensor integration, this parameter alone does not fully describe the deformation capability of the soft robotic system. To provide a more comprehensive assessment, finite element simulations were performed to compare the deformation behavior of the soft robotic structure with and without the integrated sensing layer, and to evaluate the effective strain experienced by the sensor (Figure 4).

The von Mises stress maps reported in Figure 4a,b show the progressive deformation experienced by the soft robotic structure as the applied displacement increases up to 4 mm, with stress concentrations localized in the bending region beneath the indenter. Images also highlight the different stress distributions in the soft robotic structure without (Figure 4a) and with (Figure 4b) the sensing platform over the time of simulation. The reaction force exerted by the structure was 2.77 mN in the absence of the sensor and 8.90 mN after integration (Figure 4c), in good agreement with the experimental results reported in Figure 3c.

A more detailed analysis of the mechanical stimulus experienced by the sensing platform of the catheter was carried out by extracting the longitudinal strain at selected points, which corresponds to the sensor location (Figure 4d). The results indicate a spatial gradient in strain distribution, with the highest strain values observed at Node 1, located in the outermost region of the bend, and progressively lower values at Nodes 2 and 3. Importantly, the maximum strain levels remain within a moderate range (≈1–2.5%) for the applied displacement, corresponding to a bending angle of approximately 30°, confirming that the sensing layer operates within a regime suitable for reliable electromechanical transduction [29]. These findings suggest that, although the integration of the sensing element leads to a measurable increase in stiffness, the functional compliance of the soft robotic system is preserved, as the device retains its ability to achieve the intended bending behavior under controlled actuation.

2.3 | Electromechanical Characterization of Sensorized Soft Robots

Electromechanical characterization of the soft robotic systems consists in the application of controlled deformation by means of an indenter, and the recording of the variation of the OFET output current. The working principle of OFETs as strain sensors is well documented: small molecule semiconductors forming polycrystalline films respond to an applied deformation with a modification of crystalline domains distribution [30, 31]. This affects electrical parameters, in particular charge carrier mobility, which reduces if the applied deformation induces an elongation of the film, and increases in the case of compression. All in all, a modification of the output current is obtained, proportionally to the applied percentage strain $\varepsilon_{\%}$ according to the formula:

$$\varepsilon_{\%} = \frac{t_{sub}}{2R}$$

being t_{sub} the thickness of the substrate, and R the bending radius. This particular formulation is valid if the substrate thickness and Young's modulus are much larger than those of the device. In this assembly, t_{sub} is, at the best case, the thickness of the silicone cylinder's walls (of about 300 μm): therefore, even if the micrometrical-thick Parylene C substrate is more rigid than the soft robotic system, the last equation can be considered valid due to the significant difference of thicknesses.

In order to apply a controlled deformation, a linear motor platform was employed to apply a displacement, similarly to the protocol followed in the mechanical characterization. The deformation profile generated by the linear actuator from the displacement (from 1 to 6 mm) results in bending angles ranging from 5° to 30°, as shown in Figure S5. Such a deformation range was chosen as representative of different operational scenarios of the soft robotic system as a sensorized catheter tip for endoscopic applications, such as the drug delivery in the liver small vessels system [32].

The transistor output current was recorded in real-time, at fixed values for drain-to-source voltage V_{DS} and gate-to-source voltage V_{GS}. Results are shown in Figure 5a, which reports the current variation $\Delta I = I_{bent} - I_{flat}$, being I_{bent} the current of the transistor

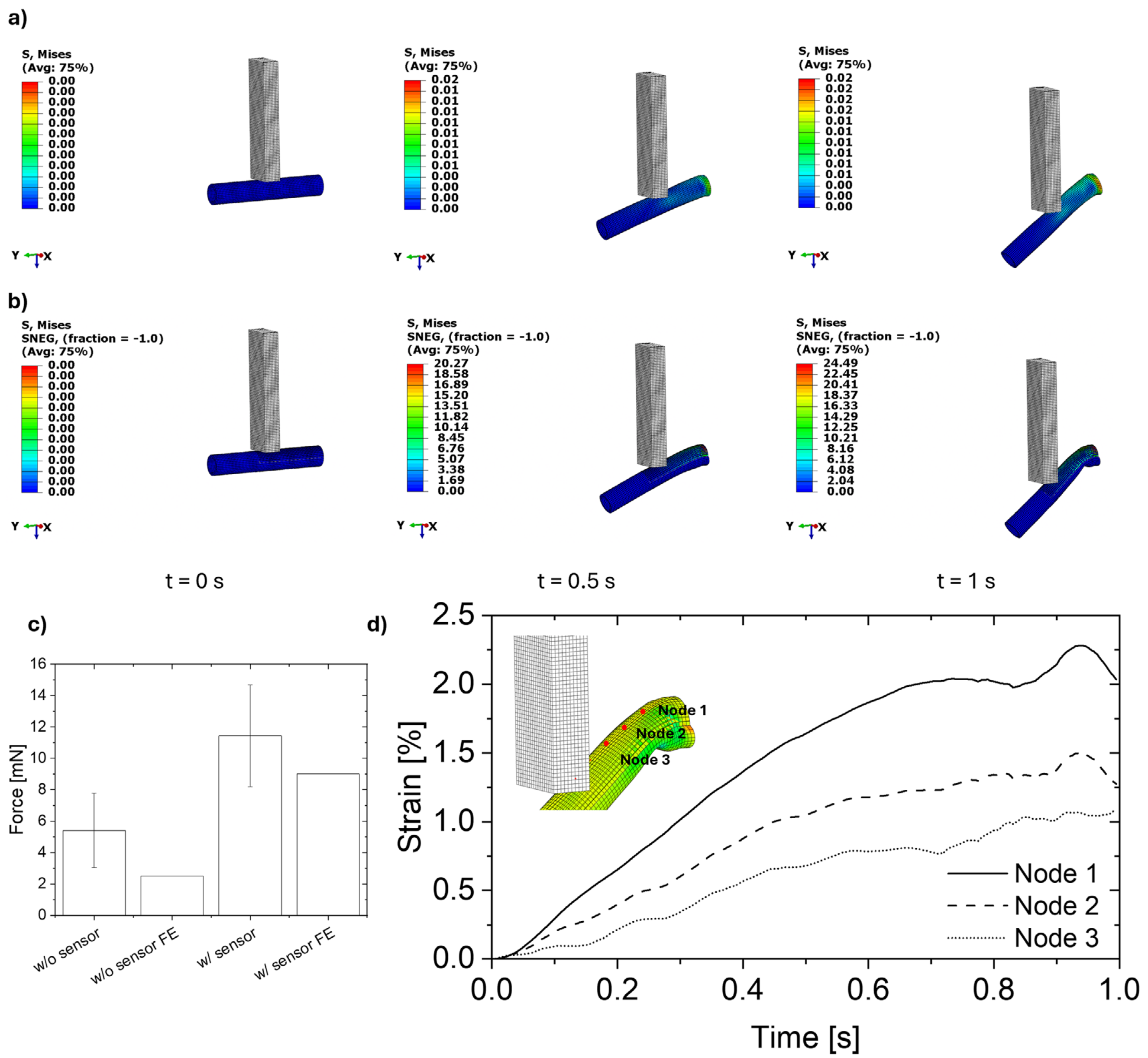

FIGURE 4 | Finite element (FE) simulation of the experiment. (a) soft robotic platform alone; (b) soft robotic platform with integrated sensing platform. Contour maps of the Von Mises stress distribution within the samples are shown for both configurations at three selected time points (0, 0.5, and 1 s). (c) Comparison between experimental results and FE simulations presented as a bar chart. (d) FE simulation results showing the time evolution of strain at three selected nodes of the sensing platform. The inset magnification highlights the nodes that were evaluated.

during the application of the deformation, and I_{flat} the baseline current in the undeformed state. This allows a direct comparison between performances obtained at different values of the gate voltage, resulting in different values of the I_{flat}: in particular, responses at $V_{GS} = 0\ V$ (i.e., device barely switched on) and $V_{GS} = -5\ V$ (i.e., device fully switched on in saturation regime) are reported. It is possible to observe that, for both gate polarizations, a clear current variation is observed for the different applied deformations, in a way that results proportional to the extent of the soft robot deflection. When deformation is removed, the current comes back to I_{flat} value, that is well maintained upon the duration of the whole experiment (see Figure S6) for all considered values of V_{GS}. Interestingly enough, the increased overthreshold voltage $V_{GS} - V_{TH}$ results in an increase in the sensor response to a given deformation: since charge carrier mobility is a function of the gate voltage, a larger overthreshold condition is related to higher values of mobility, which are thus more prone to be affected by morphological changes induced by the deformation. Therefore, a larger modification of the transistor output current is expected. Such a result is well explained by calibration curves shown in Figure 5b, reporting current variation as a function of the derived bending angles for five different values of gate voltages (corresponding current vs. time recordings are shown in Figure S5). When the device is barely in the on state, the current variation is relatively low, even in the case of significant bending, and shows a sub-linear dependence on applied bending angles. The more the device is switched on, the more linear and significant is the current variation. As a consequence, sensitivity to applied deformation (i.e., the slope of the calibration curve extrapolated in its linear range) increases with the overthreshold,

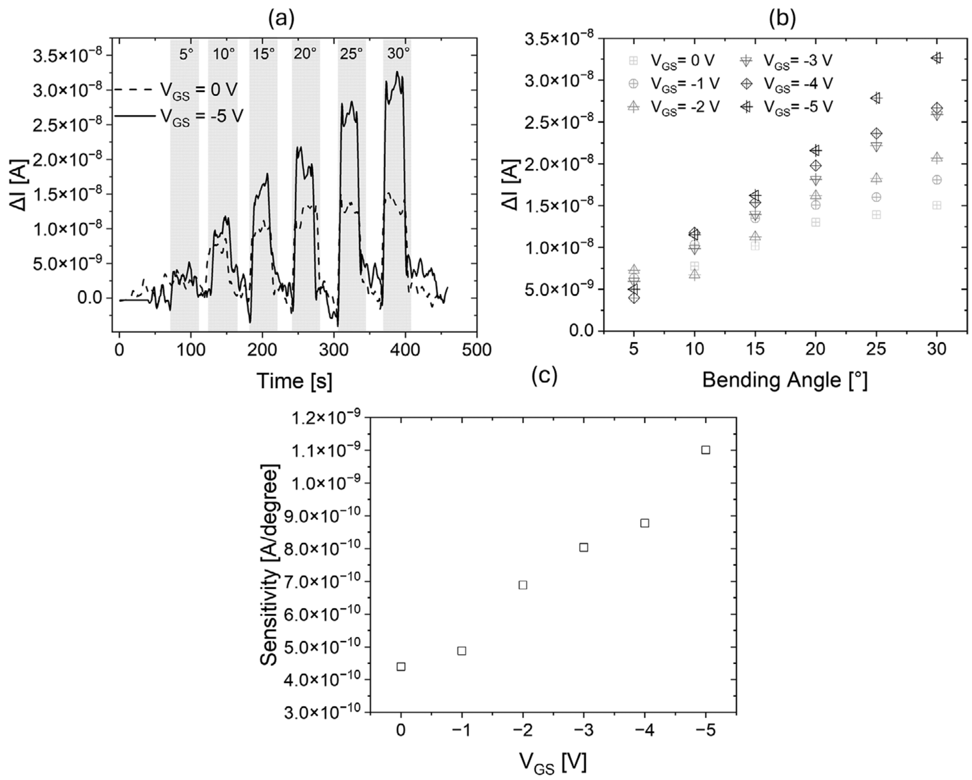

FIGURE 5 | Electromechanical characterization of ultra-flexible OFETs in soft robotic applications: (a) representative real-time current variation during the application of deformation at six different bending radius in a catheter hosting OFET strain sensors for two different gate voltages ($V_{GS} = 0\ V$, dashed line; $V_{GS} = -5\ V$, solid line) and for $V_{DS} = -5\ V$; (b) calibration curves as current variation vs. bending angle for different values of V_{GS} ranging from 0 to -5 V; the inset shows the sensitivity (slope of the calibration curves in the linear range) as a function of the gate voltage.

reaching values exceeding 1 nA per degree of deformation (inset in Figure 4b), which is fully compatible with effective electronic readout. It is noteworthy that the profile of the calibration curve well resembles the force vs. displacement analysis shown in Figure 3c, thus making it possible a direct correlation between the entity of the current variation and the force responsible of the displacement. This aspect is fundamental for future application of the sensorized soft robotic system in configurations including an actuating element, such as piezoelectric, pneumatic or even biohybrid elements [19, 25].

2.4 | Electromechanical and Environmental Stability of the Sensorized Catheter

The envisaged application of the sensorized soft robotic system in endoscopic applications poses important challenges in terms of performance stability and reproducibility in a harsh environment. Although the overall electrical stability of the proposed OFET technology has been previously demonstrated, considering fundamental parameters such as temperature [33], a deeper investigation into the peculiar conditions of mechanical operation in the human body is needed.

In particular, two main aspects have been considered: mechanical stress, such as repeated application of large deformations for a prolonged time, and the effect of the liquid environment. Figure 6a shows the result of the application of 140 bending cycles at an estimated bending radius of about 30° over a time period of 1200 s. This timing was chosen to optimize the sampling frequency of the employed machinery, thus making possible an analysis of the single force applications: the results on a reduced interval of 100 s is shown in the inset to the Figure. During the experiment, the sensor was biased in full ON conditions (V_{GS} = -4 V, V_{DS} = -5 V), i.e., at the most severe conditions in terms of bias stress and thus baseline drift. The output current shown in the plot demonstrates that both the sensor baseline current and response to deformations are well reproducible along the whole experiment. In particular, baseline current shifts of about 8%; variability in the timing and extent of the response (clearly evident in the inset to the Figure) can be justified with the fact that the deformation was applied using an open-loop mechanical indenter, i.e., with a limited control on the actual amount of force applied in each deformation.

Figure 6b shows the output current of a sensorized soft robot, partially immersed in a Beaker containing a 0.9X commercial phosphate buffer saline (PBS) solution. At the beginning, the device was kept in dry conditions: it is possible to observe an initial drift and then a stabilization of the output current. This drift is typically related to the charge of the capacitive structures in the OFET device. After an acceptable stabilization had been reached, the device was partially inserted in the Beaker, in order to have the OFET active area totally immersed in the liquid environment. The immersion activated another drift dynamic, which reached a substantial plateau after 200 s, leaving to a minimum current reduction in time. This result is mainly related to the characteristics of Parylene C as a coating layer: its hydrophobicity

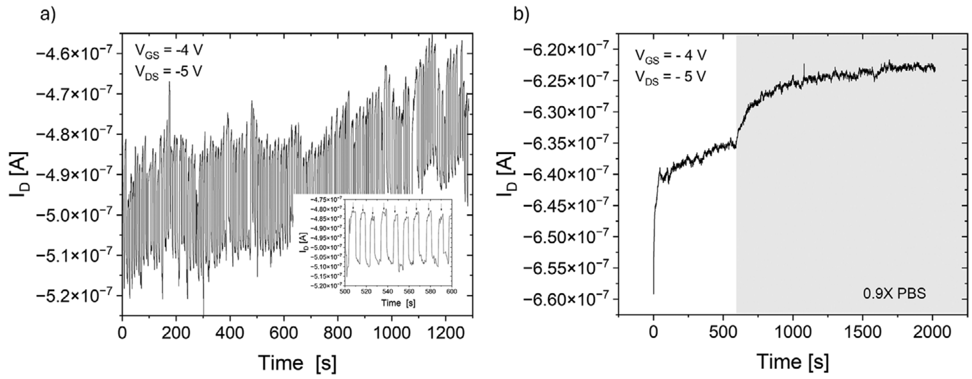

FIGURE 6 | (a) Electromechanical stability test of sensorized soft robot subjected to 140 consecutive deformations at 30°; the inset shows a subset of 100 s in the experiment. (b) Stability of the electrical performances in time, in dry conditions, and with the device immersed in a 0.9X PBS solution. In both experiments, device polarization was V_{DS} = -5 V and V_{GS} = -4 V.

and capability of forming pinhole-free and conformal coatings ensure prolonged lifetime even in the presence of high humidity and strong ionic concentrations.

3 | Conclusions

In this work, a novel approach to sensorize a soft robotic structure through the integration of a flexible electronic sensing system is proposed. The sensing system is based on an all-organic, ultra-flexible OFET strain sensor, entirely fabricated by means of large area techniques, with mechanical properties compatible with soft robotic applications. The system was firmly embedded within a hollow silicone-based structure, preserving its electrical performance, mechanical compliance, and softness during bending, as demonstrated by a thorough mechanical analysis. Electromechanical characterization allowed the evaluation of the correct system functionality along a wide deformation range, compatible with future application of the sensorized system in an endoscopic drug delivery application. Moreover, programmability of the sensing performance was characterized, further improving the flexibility of the proposed approach in different experimental conditions. Preliminary mechanical and environmental stress tests allowed demonstrating the stability of the sensing performance even upon multiple deformations and prolonged exposure to harsh conditions.

This work opens new avenues for introducing proprioception in soft robots through a minimally invasive flexible electronics technology, and paves the way to future exploitation in applications scenarios by the integration of actuation systems, such as biohybrid actuators, ensuring a real-time evaluation of robot movement toward continuous observability and controllability.

4 | Experimental Section

4.1 | Flexible Sensors Fabrication and Electrical Characterization

Ultra-flexible OFETs designed for catheter integration were fabricated using a bottom-gate, bottom-contact architecture, selected for its mechanical robustness and suitability for strain-sensing applications. A 250 µm-thick polyethylene naphthalate (PEN) film served as the supporting substrate. A thin sacrificial layer of polyvinyl alcohol (PVA) was spin-coated onto the PEN and subsequently cured on a hot plate at 90°C for 10 min to ensure uniform coverage and strong adhesion.

Parylene C was chosen as an ultra-flexible substrate for the sensor for its biocompatibility, hemocompatibility, dielectric stability, and smooth surface, which together promote reliable multilayer integration. A 500 nm-thick Parylene C layer was deposited on PVA-coated supports via chemical vapor deposition (CVD) using a PDS 2010 Labcoter 3 (Specialty Coating System).

A SUSS LP50 inkjet printer (PiXDRO) and a 12-nozzle cartridge with a single drop volume of 2.4 pL (Samba, Fujifilm Dimatix) were employed for patterning gate, source, and drain contacts. A commercial ink (Clevios PJET HC, Heraeus) based on Poly(3,4-ethylenedioxythiophene) polystyrene sulfonate (PEDOT:PSS) was used for the whole transistor structure. Patterns were printed at a platen temperature of 60°C with a resolution of 1270 dpi, adapting their thickness (i.e., number of layers) and other printing conditions (e.g., number of nozzles, jetting frequency) to the different resolution needs. Specifically, gates were inkjet-printed directly on the Parylene C surface using two layers of PEDOT:PSS, with a width of 1 mm, and dried on the printer platen. Then, a 300 nm-thick Parylene C layer was deposited by CVD to serve as the gate dielectric, using an adhesion promoter (A-174 Silane, Specialty Coating Systems) to improve the quality of the film. Source and drain electrodes were inkjet printed on top of the gate insulator, using two layers for the channel area (interdigitated shape, nominal aspect ratio of 60), and dried on a hot plate at 90°C for 15 min to reduce solubility of the printed tracks into solvents. To this aim, an ethylene glycol (EG, Sigma–Aldrich) layer was printed afterward on the channel areas and let dry on the platen at 60°C. A (6,13-bis(triisopropylsilylethynyl)pentacene (TIPS-pentacene, Sigma–Aldrich) solution (1.5wt.% in anisole anhydrous) was drop-cast across the transistor channels to form the active layer. A volume of 0.5 µL was dispensed through a micropipette, and let dry in a fume hood for 15 min at room-temperature. Finally, devices were encapsulated with a 0.7 µm-thick layer of Parylene to provide a final biocompatible and hemocompatible surface. The sensor dimensions were adapted to the soft robotic platform geometry, with an overall area of 9.2 mm × 4 mm.

4.2 | Soft Robotic Platform Fabrication

The soft robotic platform was fabricated in accordance with the protocol reported by Bartolucci et al. [25]. A silicone blend composed of polydimethylsiloxane (PDMS, Sylgard 184 Silicone Elastomer kit, Dow Corning) and EcoFlex 00–10 (Smooth-On) in a 1:10 ratio, prepared without the PDMS curing agent, was selected for molding. The molds were designed in Autodesk Fusion (Autodesk) to produce cylindrical samples with an internal diameter of 2 mm and a wall thickness of 0.3 mm. They were fabricated via SLA 3D printing (Form 3B+, Formlabs) using a surgical guide resin (Formlabs) and subsequently assembled to form the negative cavity for casting. The silicone mixture was injected into the assembled molds using two syringes and cured in an oven for 1.5 h at 50°C. After thermal curing, the samples were left at room-temperature overnight to complete polymerization. The following day, the molds were opened, and the soft robotic structures were carefully extracted.

4.3 | Flexible Electronic Platform Integration on the Soft Robotic Platform

The adhesion between the sensor and the soft robotic structures was ensured by applying a thin layer of uncured silicone blend at the sensor attachment site through localized thin-layer coating using a fine applicator. To ensure precise alignment between the sensor and the soft robotic components, a dedicated setup was developed, enabling sensor placement with minimal misalignment (Figure S1).

4.4 | Mechanical Characterization

Mechanical characterization of the soft robotic platform, both with and without the integrated electronic platform, was performed using a universal testing machine (Instron 5965, 10 N load cell, Instron, Norwood, MA, USA). Two custom 3D-printed elements were mounted between the machine clamps to ensure proper alignment of the samples. The soft robotic structures were positioned on the lower fixture, while an indenter (contact area: 8 mm^2) attached to the upper fixture was used to apply the controlled displacement of 0.5 mm s^{-1}, up to 4 mm. The complete experimental setup is shown in Figure S4. For each experimental condition, four independent samples were tested, and three measurements were performed for each sample. The mean values were calculated across the technical replicates, and the resulting mean and standard deviation values from the four samples were then used to graph the overall curve. Simple linear regressions were calculated from each force-displacement curve to extract the spring constant value (N/m) for each sample.

4.5 | Electromechanical Characterization

A custom experimental setup reproducing the configuration of the Universal Testing Machine was developed. The system incorporated a precision linear stage (VT-80 Linear Stage, PI) to apply controlled displacements to the samples. Four soft robotic structures integrated with the flexible electronic film were tested. Each sample was mounted on a 3D-printed holder, while a 3D-printed rigid indenter positioned on the opposite side was used to exert the desired displacement to achieve an approximate angle of 30°. The testing parameters were identical to those employed in the mechanical characterization performed with the Universal Testing Machine. The complete setup is illustrated in Figure S4.

4.6 | Finite Element Analysis

The investigation of the mechanical response of the soft robotic system and the sensor-integrated system was performed through FE analysis using the commercial software Abaqus 2020 (Dassault Systems).

A controlled displacement was applied to the device to determine the reaction force exerted along the vertical axis (*Fz*), consistently with the experimental configuration. More specifically, the displacement was imposed on a reference point located at the center of the indenter's lower surface, at the interface with the soft robotic system; this configuration corresponds to the loading conditions adopted in the experimental setup (i.e., 7.5 mm from the constrained extremity). The reference point was kinematically coupled to the corresponding surface of the structure to ensure uniform load transfer. A boundary condition was applied to constrain one extremity of the soft robotic structure, reproducing the experimental conditions provided by the support pin used during mechanical testing (as reported in Figure S7).

The PDMS-EcoFlex blend used to fabricate the soft robotic structure was modeled as a hyperelastic material through the Ogden model. The constitutive behavior was defined by fitting the stress–strain experimental curve, which was implemented in Abaqus as material input, following a procedure similar to that reported in Bartolucci et al. [25]. The sensor was modeled as a linear elastic layer with mechanical properties representative of Parylene C, assuming a homogeneous and isotropic behavior. Its thickness was defined consistent with the height of Parylene C in the experimental device (e.g., 1.5 µm). The contact between the soft robotic structure and the sensor was set as a "tie constraint" to ensure full adhesion and no relative sliding between the two components during deformation, thus mimicking the strong interfacial bonding.

A structured mesh based on quadrilateral elements (C3D8R: An 8-node linear brick, reduced integration, hourglass control) was implemented for both the soft structure and the sensor layer, with an element size of 0.2 mm. A mesh convergence analysis was performed by progressively refining the mesh size until variations in the computed reaction force were below a predefined threshold ($\leq$ 15%) to determine numerical stability and the accuracy of the results (Figure S8).

The simulations were carried out using the Abaqus/Explicit solver, applying a ramp loading rate.

The strain distribution within the sensor was extracted from the finite element simulations to evaluate the mechanical stimulus experienced by the sensing layer. In particular, the logarithmic strain component along the longitudinal direction of the sensor length (LE22) was considered. This metric was selected as it provides an accurate description of strain under large deformation conditions, which are typical of soft robotic systems. For each simulation, the strain perceived by the sensor was quantified by extracting the spatial distribution of LE22 over 5 sensor nodes and computing the values over time. This approach enabled the estimation of the strain effectively transferred to the sensing element.

4.7 | Statistical Analysis

A normality test (D'Agostino-Pearson) was performed on all experimental data to assess data distribution. Then, the data were analyzed based on their type of distribution, as described in the figure captions. Statistical analyses were carried out using GraphPad Prism (v 9). The significance threshold was set at 5%.

Acknowledgements

The authors gratefully acknowledge the European Union's Horizon Europe research and innovation programme for funding the project BIOMELD under grant agreement No. 101070328.

Open access publishing facilitated by Universita degli Studi di Cagliari, as part of the Wiley - CRUI-CARE agreement.

Funding

"BioMeld—A Modular Framework for Designing and Producing Biohybrid Machines" (European Union's Horizon Europe research and innovation Programme, grant agreement No. 101070328).

Conflicts of Interest

The authors declare no conflicts of interest.

Data Availability Statement

The data that support the findings of this study are available from the corresponding author upon reasonable request.

References

1. C. Laschi, B. Mazzolai, and M. Cianchetti, "Soft Robotics: Technologies and Systems Pushing the Boundaries of Robot Abilities," *Science Robotics* 1, no. 1 (2016): aah3690, https://doi.org/10.1126/scirobotics.aah3690.

2. W. Dou, G. Zhong, J. Cao, Z. Shi, B. Peng, and L. Jiang, "Soft Robotic Manipulators: Designs, Actuation, Stiffness Tuning, and Sensing," *Advanced Materials Technologies* 6, no. 9 (2021): 2100018, https://doi.org/10.1002/admt.202100018.

3. S. Zaidi, M. Maselli, C. Laschi, and M. Cianchetti, "Actuation Technologies for Soft Robot Grippers and Manipulators: A Review," *Current Robotics Reports* 2 (2021): 355–369, https://doi.org/10.1007/s43154-021-00054-5.

4. Y. Qiu, A. Ashok, C. C. Nguyen, Y. Yamauchi, T. N. Do, and H.-P. Phan, "Integrated Sensors for Soft Medical Robotics," *Small* 20, no. 22 (2024): 2308805, https://doi.org/10.1002/smll.202308805.

5. C. Hegde, J. Su, J. M. R. Tan, K. He, X. Chen, and S. Magdassi, "Sensing in Soft Robotics," *ACS Nano* 17, no. 16 (2023): 15277–15307, https://doi.org/10.1021/acsnano.3c04089.

6. M. Eder, F. Hisch, and H. Hauser, "Morphological Computation-based Control of a Modular, Pneumatically Driven, Soft Robotic Arm," *Advanced Robotics* 32, no. 7 (2018): 375–385, https://doi.org/10.1080/01691864.2017.1402703.

7. H. Hauser, T. Nanayakkara, and F. Forni, "Leveraging Morphological Computation for Controlling Soft Robots: Learning From Nature to Control Soft Robots," *IEEE Control Systems* 43, no. 3 (2023): 114–129, https://doi.org/10.1109/MCS.2023.3253422.

8. H. Wang, M. Totaro, and L. Beccai, "Toward Perceptive Soft Robots: Progress and Challenges," *Advanced Science* 5, no. 9 (2018): 1800541, https://doi.org/10.1002/advs.201800541.

9. M. Sanati, A. Sandwell, H. Mostaghimi, and S. S. Park, "Development of Nanocomposite-Based Strain Sensor With Piezoelectric and Piezoresistive Properties," *Sensors* 18, no. 11 (2018): 3789, https://doi.org/10.3390/s18113789.

10. G. Mariotti and L. Vannozzi, "Fabrication, Characterization, and Properties of Poly (Ethylene-Co-Vinyl Acetate) Composite Thin Films Doped With Piezoelectric Nanofillers," *Nanomaterials* 9, no. 8 (2019): 1182, https://doi.org/10.3390/nano9081182.

11. J. Jung, M. Park, D. Kim, and Y.-L. Park, "Optically Sensorized Elastomer Air Chamber for Proprioceptive Sensing of Soft Pneumatic Actuators," *IEEE Robotics and Automation Letters* 5, no. 2 (2020): 2333–2340, https://doi.org/10.1109/LRA.2020.2970984.

12. M. Alshawabkeh, H. Alagi, S. E. Navarro, et al., "Highly Stretchable Additively Manufactured Capacitive Proximity and Tactile Sensors for Soft Robotic Systems," *IEEE Transactions on Instrumentation and Measurement* 72 (2023): 1–10, https://doi.org/10.1109/TIM.2023.3250232.

13. H. Kwon, Y. Yang, G. Kim, D. Gim, and M. Ha, "Anisotropy in Magnetic Materials for Sensors and Actuators in Soft Robotic Systems," *Nanoscale* 16, no. 14 (2024): 6778–6819, https://doi.org/10.1039/D3NR05737B.

14. G. De Luca, A. C. Bressi, R. Pathan, et al., "Soft Robots Proprioception Through Stretchable Laser-Induced Graphene Strain Sensors," *Advanced Intelligent Systems* 7, no. 10 (2025): 2401071, https://doi.org/10.1002/aisy.202401071.

15. J. Qu, G. Cui, Z. Li, et al., "Advanced Flexible Sensing Technologies for Soft Robots," *Advanced Functional Materials* 34, no. 29 (2024): 2401311, https://doi.org/10.1002/adfm.202401311.

16. Y. Jia, Y. Wu, Y. Chen, T. Hua, and H. Le, "Characterization and Modelling of Carbon Black Nanocomposite Strain Sensor on Pneumatic Driven Flexible Catheter for Pulmonary Surgery Robots," *Materials & Design* 248 (2024): 113512, https://doi.org/10.1016/j.matdes.2024.113512.

17. J. Shang, X. Ma, P. Zou, et al., "A Flexible Catheter-based Sensor Array for Upper Airway Soft Tissues Pressure Monitoring," *Nature Communications* 16, no. 1 (2025): 287, https://doi.org/10.1038/s41467-024-55088-y.

18. K. Wang, Z. Wu, R. Wu, et al., "Direct Fabrication of Flexible Strain Sensor With Adjustable Gauge Factor on Medical Catheters," *Journal of Science: Advanced Materials and Devices* 8, no. 3 (2023): 100558, https://doi.org/10.1016/j.jsamd.2023.100558.

19. S. Lai, J. Fuentes, M. Guix, G. Casula, P. Cosseddu, and S. Sánchez, "Real-Time Force Monitoring of Electrically Stimulated 3D-Bioengineered Muscle Bioactuators Using Organic Sensors With Tunable Sensitivity," *Advanced Intelligent Systems* 7, no. 10 (2025): 2400407, https://doi.org/10.1002/aisy.202400407.

20. M. Concas, A. Mascia, S. Lai, A. Bonfiglio, and P. Cosseddu, "Fabrication of Flexible Double-Gate Organic Thin Film Transistor For Tactile Applications," *Advanced Materials Technologies* 9, no. 22 (2024): 2400534, https://doi.org/10.1002/admt.202400534.

21. D. Braga and G. Horowitz, "High-Performance Organic Field-Effect Transistors," *Advanced Materials* 21, no. 14–15 (2009): 1473–1486, https://doi.org/10.1002/adma.200802733.

22. L. Vannozzi, L. Ricotti, M. Cianchetti, et al., "Self-assembly of Polydimethylsiloxane Structures From 2D to 3D for Bio-hybrid Actuation," *Bioinspiration & Biomimetics* 10 (2015): 056001, https://doi.org/10.1088/1748-3190/10/5/056001.

23. L. Vannozzi, A. Lucantonio, A. Castillo, A. De Simone, and L. Ricotti, "Modeling Self-Rollable Elastomeric Films for Building Bioinspired Hierarchical 3D Structures," *International Journal of Molecular Sciences* 23, no. 15 (2022): 8467, https://doi.org/10.3390/ijms23158467.

24. S. Lai, A. Zucca, P. Cosseddu, F. Greco, V. Mattoli, and A. Bonfiglio, "Ultra-conformable Organic Field-Effect Transistors and Circuits for Epidermal Electronic Applications," *Organic Electronics* 46 (2017): 60–67, https://doi.org/10.1016/j.orgel.2017.03.038.

25. A. Bartolucci, J. Fuentes, D. Guarnera, et al., "Monolithic Biohybrid Flexure Mechanism Actuated by Bioengineered Skeletal Muscle Tissue," *Advanced Intelligent System* 7, no. 10 (2025): 2400989, https://doi.org/10.1002/aisy.202400989.

26. E. Zhu, P. Mandal, and C. R. Calladine, "Buckling of Thin Cylindrical Shells: An Attempt to Resolve a Paradox," *International Journal of Mechanical Sciences* 44, no. 8 (2002): 1583–1601, https://doi.org/10.1016/S0020-7403(02)00065-6.

27. L. Vannozzi, T. Mazzocchi, A. Hasebe, S. Takeoka, T. Fujie, and L. Ricotti, "A Coupled FEM-SPH Modeling Technique to Investigate the Contractility of Biohybrid Thin Films," *Advanced Biosystems* 4, no. 8 (2020): 1900306, https://doi.org/10.1002/adbi.201900306.

28. D. R. Yao, I. Kim, S. Yin, and W. Gao, "Multimodal Soft Robotic Actuation and Locomotion," *Advanced Materials* 36, no. 19 (2024): 2308829, https://doi.org/10.1002/adma.202308829.

29. M.-Z. Li, L.-C. Guo, G. Liu, et al., "Manipulating Strain in Transistors: From Mechanically Sensitive to Insensitive," *Advanced Electronic Materials* 8 (2022): 2101288, https://doi.org/10.1002/aelm.202101288.

30. P. Cosseddu, S. Milita, and A. Bonfiglio, "Strain Sensitivity and Transport Properties in Organic Field-Effect Transistors," *IEEE Electron Device Letters* 33, no. 1 (2011): 113–115, https://doi.org/10.1109/LED.2011.2173898.

31. P. Cosseddu, G. Tiddia, S. Milita, and A. Bonfiglio, "Continuous Tuning of the Mechanical Sensitivity of Pentacene OTFTs on Flexible Substrates: From Strain Sensors to Deformable Transistors," *Organic Electronics* 14, no. 1 (2013): 206–211, https://doi.org/10.1016/j.orgel.2012.10.033.

32. C. Salvatori, D. Trucco, I. Niosi, L. Ricotti, and L. Vannozzi, "A Novel Steerable Catheter Controlled With a Biohybrid Actuator: A Feasibility Study," in Conference on Biomimetic and Biohybrid Systems, (Springer Nature Switzerland, 2023), 378–393, https://doi.org/10.1007/978-3-031-39504-8_26.

33. G. Casula, P. C. Ricci, P. Cosseddu, G. Mura, and S. Lai, "Enhancing Thermal and Radiation Hardness of All-Organic Printed Transistors by a Flexible and Transparent Encapsulation Layer for Low Earth Orbit Applications," *Physica Status Solidi (a)* 222 (2025): 2500381, https://doi.org/10.1002/pssa.202500381.

Supporting Information

Additional supporting information can be found online in the Supporting Information section.

Supporting File: aelm70420-sup-0001-SuppMat.docx.